ACS APPLIED MATERIALS & INTERFACES

www.acsami.org

Research Article

F-Center-Mediated Growth of Patterned Organic Semiconductor Films on Alkali Halides

Darius Günder, Valentin Diez-Cabanes, Andrea Huttner, Tobias Breuer, Vincent Lemaur, Jérôme Cornil, and Gregor Witte*

Cite This: *ACS Appl. Mater. Interfaces* 2022, 14, 46086−46094

Read Online

ACCESS | Metrics & More | Article Recommendations | Supporting Information

ABSTRACT: Organic semiconductors combine flexible tailoring of their optoelectronic properties by synthetic means with strong light−matter coupling, which is advantageous for organic electronic device applications. Although spatially selective deposition has been demonstrated, lateral patterning of organic films with simultaneous control of molecular and crystalline orientation is lacking as traditional lithography is not applicable. Here, a new patterning approach based on surface-localized F-centers (halide vacancies) generated by electron irradiation of alkali halides is presented, which allows structural control of molecular adlayers. Combining optical and atomic force microscopy, X-ray diffraction, and density functional theory (DFT) calculations, it is shown that dinaphthothienothiophene (DNTT) molecules adopt an upright orientation on pristine KCl surfaces, while the F-centers stabilize a recumbent orientation, and that these orientations are maintained in thicker films. This specific nucleation results also in different crystallographic morphologies, namely, densely packed islands and jagged fibers, each epitaxially aligned on the KCl surface. Spatially selective surface irradiation can also be used to create patterns of F-centers and thus laterally patterned DNTT films, which can be further transferred to any (including elastomer) substrate due to the water solubility of the alkali halide growth templates.

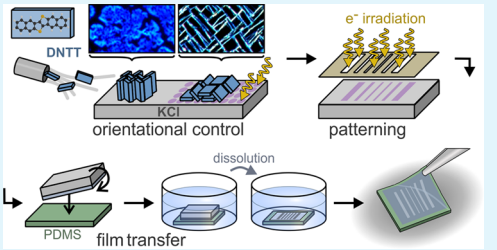

KEYWORDS: *DNTT, organic semiconductors, film patterning, color center, density functional theory*

1. INTRODUCTION

Organic electronics is a rapidly growing field of interest which promises cost-effective and low-temperature device processing, even enabling the realization of flexible electronic devices.[1,2] A particular advantage of organic semiconductors and chromophores is the tailoring of their electronic properties through targeted synthesis instead of laborious band structure engineering necessary for inorganic semiconductors. However, device processing also requires lateral structuring and patterning of the semiconducting films, which remains challenging for molecular materials since photolithography is not applicable due to the radiation sensitivity and lack of chemical robustness in the etching process of these materials, causing their degradation.[3] Therefore, alternative approaches are necessary, which are based on a spatially selective deposition (using shadow masks, inkjet or gravure printing[3−5]), controlled nucleation on pre-structured substrates (using inorganic surface patterns[6] or printed self-assembled monolayers[7]), or subsequent removal of material (by means of molding,[8] laser ablation,[9] or nanoscratching[10]). In addition, control of the molecular aggregation and patterning of films by laser illumination during the deposition was also demonstrated, which is caused either by local heating of the substrate surface[11] or by suppression of specific domains due to orientation-selective optothermal heating.[12] In view of the anisotropic optoelectronic properties of molecules and crystalline molecular solids, controlling the molecular and crystalline orientation of such functional films is also an important requirement to exploit this anisotropy. While orientation control is typically not possible when printing molecular layers, this can be achieved by vapor deposition of molecular films onto suitable substrate surfaces (such as oxides, metals, salts, and two-dimensional (2D) materials) and by exploiting template effects.[13] This approach often also yields epitaxial molecular films on crystalline inorganic substrates[14,15] and sometimes even leads to new, interface-stabilized phases.[16] While such template-mediated growth works well on uniform substrate surfaces, laterally structured molecular adlayers also require patterned template substrates, which poses quite a challenge when aiming to use (single) crystalline templates. In a more general context, the challenge of patterning van der Waals bound molecular materials and heterostructures is that, due to their low interaction strength, small modifications or additional interactions can have significant structural implica-

Received: August 3, 2022
Accepted: September 21, 2022
Published: October 3, 2022

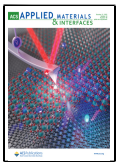

tions that are so far incompletely understood and hardly predictable.

Here, we present a novel patterning method based on the controlled generation of surface-localized F-centers (halide vacancies) on alkali halide substrates created by electron or X-ray irradiation, which affects the molecular orientation upon nucleation and thereby also the resulting film structure in a controlled manner. For the newly available organic semiconductor dinaphthothienothiophene (DNTT), which combines distinct chemical inertness with high charge carrier mobility[17−20] and thus represents a prototypical material, we demonstrate that it forms (001)-oriented films on KCl(100) surfaces, in which molecules adopt an upright orientation, while DNTT molecules adopt a recumbent orientation on irradiated KCl surfaces and form characteristic jagged fibers. Remarkably, both adlayer structures are epitaxial but with different alignments on the KCl substrate. The epitaxial order of fibers on irradiated KCl(100) is possible because the formed chlorine vacancies are localized at specific lattice sites and do not disrupt the surface periodicity, as evidenced by accompanying low-energy electron diffraction (LEED) measurements. Theoretical analysis within the framework of van der Waals-corrected density functional theory (DFT) confirms the energetic stabilization of recumbently oriented DNTT molecules adsorbed above the halide vacancies compared to the pristine surface. Furthermore, we demonstrate that the different film morphologies, which can be patterned laterally using exposure masks, can also be transferred to other substrates, even flexible polymer substrates, by dissolving the KCl substrates.

2. RESULTS AND DISCUSSION

In Figure 1, we compare the structure of DNTT films grown on pristine and on electron-irradiated KCl(100) surfaces. In

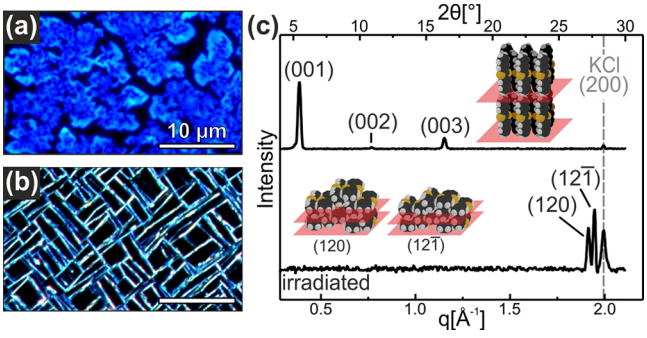

Figure 1. Optical micrographs of DNTT thin films grown on (a) pristine and (b) electron-irradiated KCl(100) surfaces, together with (c) corresponding specular X-ray diffractograms of the differently prepared films. The different molecular arrangements are depicted in the insets.

both cases, the KCl(100) surfaces are freshly cleaved, while the latter are additionally irradiated in ultrahigh vacuum (UHV) with electrons of 250 eV and a dose of 5 mC/cm^2 before DNTT deposition. On pristine KCl, the formed DNTT films consist of dendritic coalesced islands, while characteristic fibers with a length of up to 10 μm are formed on irradiated KCl. The accompanied specular X-ray diffraction measurements reveal several diffraction peaks in addition to the $(200)_{KCl}$ substrate reflection, which is identified as DNTT reflections based on a comparison with calculated powder spectra of the bulk structure (data provided in the Supporting Information).[17] The identified reflections indicate that DNTT adopts the bulk phase with a molecular herringbone packing motif on pristine and irradiated KCl substrates. In particular, we do not find any evidence of the formation of a thin-film phase upon initial growth of DNTT films on pristine KCl substrates as previously reported for SiO_2 (further information is provided in the Supporting Information).[21] However, the DNTT films exhibit quite different crystalline orientations on the differently treated KCl surfaces. On pristine KCl surfaces, (001)-oriented DNTT films are formed, in which the molecules adopt an upright orientation like on SiO_2,[22] hence reflecting a weak substrate interaction. By contrast, the crystalline fibers as observed on irradiated surfaces are oriented with their $(120)_{DNTT}$ or $(12\bar{1})_{DNTT}$ planes parallel to the KCl surface, respectively. In both crystallographic planes, DNTT molecules are oriented with their long axes nearly parallel to the substrate surface, as depicted in the inset of Figure 1c, hence reflecting a recumbent molecular orientation in stark contrast to the observed upright molecular orientation on pristine KCl substrates.

As with the film growth of other π-conjugated molecules, the degree of crystalline ordering increases with increasing substrate temperature during deposition. On pristine KCl surfaces, this is accompanied by a morphological change from a contiguous adlayer of coalesced rosette-shaped domains formed at low temperature to more discontinuous islands with increasingly straight side edges and finally the formation of separate hexagonally shaped DNTT islands at elevated temperatures (see the Supporting Information). Such temperature-induced dewetting and crystal island ripening have also been observed before for other molecular films grown on inert substrates like e.g., pentacene on SiO_2,[23] and reflects a transition from film growth to (bulk) crystal formation.[24] When increasing the substrate temperature upon growth to 365 K, which is slightly below the threshold for sublimation of multilayer films (≈385 K),[25] distinct and very smooth DNTT single crystals with diameters of more than 100 μm are formed. Transferring such an isolated DNTT crystal from the KCl growth substrate to a SiO_2 substrate (Si-wafer covered by native oxide) allows detailed in-plane X-ray diffraction (XRD) measurements and thus identification of the bordering crystallographic faces (data and details of the transfer process provided in the Supporting Information). As depicted in Figure 2a,b, the habit of such hexagonal (001)-oriented DNTT crystals exhibits characteristic angles between the bordering low-index side faces. Such characteristic angles are also observed in atomic force microscopy (AFM) micrographs of DNTT films grown at intermediate temperatures as depicted in Figure 2c, which allows an azimuthal assignment of local domains even without in-plane diffraction measurements. In addition, distinct monolayer steps of about 1.6 nm are resolved corresponding to upright standing DNTT in (001) planes with an interlayer spacing of $d_{(001)}$ = 1.62 nm. Additional information on the azimuthal alignment of DNTT films on pristine KCl on mesoscopic scale is derived from azimuthal X-ray scans using the most intense in-plane $(020)_{DNTT}$ reflection. As shown in Figure 2d, this reflection is oriented along the $\langle 001\rangle_{KCl}$ azimuth directions of the substrate appearing in four domains according to the symmetry of the KCl(100) surface. Comparing the lattice vectors of the KCl(100) and DNTT(001) planes shows a close similarity (1.7% mismatch) between the $|a_{DNTT}|$ = 6.187 Å and $|a_{KCl}| = |b_{KCl}|$ = 6.29 Å

https://doi.org/10.1021/acsami.2c13934
ACS Appl. Mater. Interfaces 2022, 14, 46086−46094

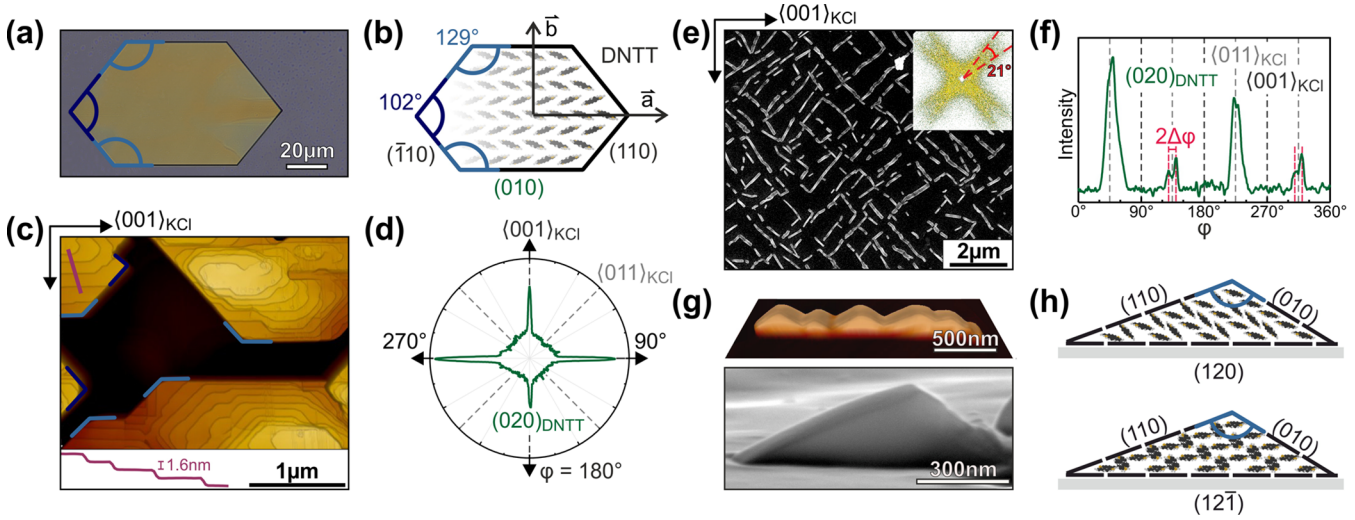

Figure 2. (a) Optical micrographs of a DNTT single crystal together with (b) a schematic representation of the molecular arrangement and the bordering crystallographic planes. (c) AFM micrograph of a DNTT film grown on nonirradiated KCl together with (d) an azimuthal in-plane X-ray scan of the $(020)_{DNTT}$ reflection. (e) Scanning electron microscopy (SEM) micrograph of DNTT fibers grown on electron-irradiated KCl. The Fourier transform analysis of the micrograph (shown in the inset) agrees well with the (f) azimuthal in-plane X-ray measurement of DNTT fibers by probing the $(020)_{DNTT}$ reflection. (g) Perspective AFM (top) and SEM (bottom) micrograph of a DNTT fiber and (h) sketch of the identified structural arrangement of DNTT molecules in the jagged fibers.

vectors, as well as a higher-order commensurability for the orthogonal direction: $|4 \times b_{DNTT}| = 30.648$ Å $\approx |5 \times b_{KCl}| = 31.45$ Å (2.6% mismatch), which explains the observed epitaxial order (for details, see the Supporting Information).

As in the case of DNTT films grown on pristine KCl(100), the shape and size of the DNTT fibers formed on the irradiated substrates also depend on the substrate temperature during deposition. For $T \leq 300$ K, only elongated clusters occur and the corresponding XRD data reveal (001) as well as (120) and (12$\bar{1}$) reflections, while at higher temperatures, exclusively fibers are formed, which increase in size with temperature but also increasingly separate (see the Supporting Information). As already visible in the optical micrograph in Figure 1b and can be seen more clearly in scanning electron microscopy (SEM) micrographs (cf. Figure 2e), the DNTT fibers are essentially oriented along the ⟨011⟩ azimuth directions of the irradiated KCl surface. However, closer inspection reveals that the fibers are not perfectly aligned along these azimuth directions but appear split. Indeed, a Fourier transform analysis of the SEM micrograph yields a splitting of the fiber direction of 21° around the high-symmetry substrate directions (cf. inset in Figure 2e). Furthermore, the tilted high-resolution SEM micrograph depicted in Figure 2g reveals that such DNTT fibers actually have a jagged structure, which is more quantitatively analyzed by AFM yielding a typical jag height of 70 nm and a fiber width of 80 nm for a DNTT film with a nominal thickness of 10 nm grown at 320 K. In addition, the quantitative analysis of the jag structure shows characteristic angles of the limiting top faces relative to the base planes (see the Supporting Information), allowing their identification as low-index $(110)_{DNTT}$ and $(010)_{DNTT}$ faces, while front and back sides are identified as $(001)_{DNTT}$ faces, as depicted in Figure 2h. Although the low intensity of in-plane reflections hampers the azimuthal analysis of thin films, this is possible for films thicker than 50 nm. As shown in Figure 2f, the polar scan of the $(020)_{DNTT}$ reflection reveals an alignment of the fibers axis along the $\langle 011 \rangle_{KCl}$ azimuths with a splitting of about 20°, thus showing their crystalline nature and confirming the fiber orientation inferred from the SEM micrographs for thin films. We note that with thicker films, the DNTT fibers coalesce (see the Supporting Information) so that their azimuthal orientation is no longer clearly visible in the microscopic images. The precise microstructural information allows us to construct a detailed model for the observed alignment of the DNTT fibers (for details, see the Supporting Information). To do this, we first determine the base vectors that span the contact plane of the two fiber orientations, resulting in $a = [001]_{DNTT}$ and $b = [2\bar{1}0]_{DNTT}$ for the (120) base plane, and $a = [101]_{DNTT}$ and $b = [\bar{2}10]_{DNTT}$ for the (12$\bar{1}$) base plane.

Next, we find that the epitaxial alignment of the fibers can be well approximated by commensurate higher-order adlayer structures on KCl, which are described by $\begin{pmatrix} 2 & 3/2 \\ 4/3 & -2 \end{pmatrix}$ and $\begin{pmatrix} 9/4 & 7/4 \\ 15/8 & -11/8 \end{pmatrix}$ superstructures for the (120)- and (12$\bar{1}$)-oriented DNTT fibers, respectively. These structures reveal again a close match with the KCl surface lattice: $|2 \times a_{DNTT}| = 32.42$ Å $\approx |4 \times a_{KCl} + 3 \times b_{KCl}| = 31.45$ Å (3.1% mismatch) and $|3 \times b_{DNTT}| = 43.65$ Å $\approx |4 \times a_{KCl} - 6 \times b_{KCl}| = 45.36$ Å (3.8% mismatch) for the (120) plane, as well as $|4 \times a_{DNTT}| = 68.4$ Å $\approx |9 \times a_{KCl} + 7 \times b_{KCl}| = 71.72$ Å (4.6% mismatch) and $|8 \times b_{DNTT}| = 116.4$ Å $\approx |15 \times a_{KCl} - 11 \times b_{KCl}| = 117.00$ Å (0.5% mismatch) for the (12$\bar{1}$) plane. In these adlayers, the fiber directions are given by the $[2\bar{1}0]_{DNTT}$ and $[\bar{2}10]_{DNTT}$ vectors for the (120) and (12$\bar{1}$) contact planes, respectively, that are rotated by −11 and +9° with respect to the $\langle 011 \rangle_{KCl}$ azimuth directions. Since fibers can also grow in the opposite stacking direction i.e., with ($\bar{1}$20) and ($\bar{1}$21) orientations leading to the formation of mirrored fiber domains, fiber axes appear aligned ±9 and ±11° around the $\langle 011 \rangle_{KCl}$ azimuth directions, which nicely corresponds to the observed splitting of about 21°.

To rationalize the experimentally observed rather different film morphologies (hexagonal islands vs jagged fibers) in terms of their energy, we further computed the surface free energies of DNTT crystals. These are associated with different

https://doi.org/10.1021/acsami.2c13934
ACS Appl. Mater. Interfaces 2022, 14, 46086−46094

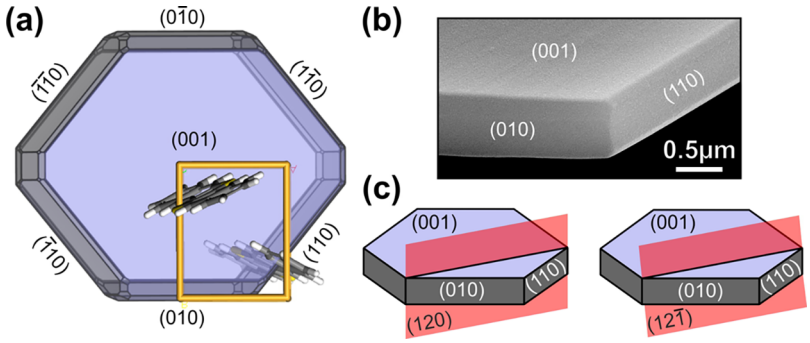

Figure 3. (a) Representation of the computed Wulff structure of a bulk DNTT crystal, together with (b) a SEM micrograph of a single-crystal corner recorded under tilted illumination to visualize the side faces and (c) a schematic representation of the (120) and (12$\bar{1}$) planes relative to the crystal habit.

crystallographic faces and thus allow us to predict the shape of an isolated DNTT single crystal. The resulting Wulff structure is displayed in Figure 3a. Rather counterintuitively, facets with higher surface energies grow faster because they provide larger binding energy for admolecules (so-called attachment energy, cf. the Supporting Information), ultimately yielding predominantly lower-surface-energy facets that determine the crystal habit. The simulated shape of the crystal fits well with the micrographs of a single crystal (cf. Figures 2a, 3b, and S7 in the Supporting Information). The theoretical analysis shows in particular that the (001) facet has the smallest surface energy (cf. Table S1) and represents the dominant facet with around 39% of the total surface. The lateral boundary faces of the crystals, oriented perpendicular to the (001) top surface, can be identified as {110}, {1$\bar{1}$0}, and {010} planes and are also seen in the magnified SEM micrograph of a DNTT crystal corner provided in Figure 3b. At first glance, the jagged fibers have a completely different morphology. However, a more detailed analysis shows that the jags correspond to the truncated corners of a hexagonal DNTT crystal (cf. Figure 3c). Since the surface of the jags is mainly given by the (001) oriented side faces and the fiber top surface corresponds to the side faces of the hexagonal islands, the surface energies are quite similar despite the supposedly different morphology.

While these analyses reveal similarities in both film morphologies, they cannot account for the origin of the jagged DNTT fibers on electron-irradiated KCl, thus requiring further consideration. Previous studies have shown that the molecular orientation and resulting structure of organic films depend sensitively on the quality of the substrate surface. For the structurally similar acenes, which also reveal a herringbone packing motif, it was found that they adopt a recumbent orientation and sometimes even form epitaxial films on highly ordered crystalline surfaces of weakly interacting substrates such as graphite, *h*BN, or MoS_2.[26−28] By contrast, on defective substrate surfaces (produced e.g., by short sputtering), the molecules instead adopt an upright orientation, yielding film surfaces of lateral densely packed molecules and low surface energy, but without any epitaxial alignment.[26−28] Notably, electron diffraction patterns recorded before and after extensive electron irradiation of the KCl(100) samples show hardly any differences (see the Supporting Information) so that a structural disorder of the substrate surface can be ruled out as an explanation for the observed fiber growth. While searching for the origin of the fiber growth, we found that a similar situation also occurs for samples irradiated with X-rays prior to DNTT deposition (see the Supporting Information). In this case, the illuminated KCl samples show a distinct blue-violet coloration. This effect is well known and reflects the formation of (bulk) F-centers due to chlorine vacancies,[29,30] which exhibit a characteristic optical signature in the optical ultraviolet/visible (UV/vis) spectra (see the Supporting Information). Since bulk F-centers can hardly affect the nucleation during film growth, it is likely that surface-localized F-centers are also formed, which we cannot optically detect separately. Interestingly, control experiments on X-ray illuminated samples, which were additionally exposed to air before DNTT deposition, show no DNTT fiber growth (see the Supporting Information); instead, well-known pyramidal adlayer structures occur that reflect (001)-oriented films as found on pristine KCl, although the samples remain purple. This indicates a quenching of the surface-localized F-centers by air contact. The formation of (bulk) F-centers is also possible by electron irradiation but requires very high energies (>100 keV).[29,31−34] However, previous work has shown that surface-localized F-centers in alkali halides are formed already by electrons with kinetic energies as low as 20 eV.[35,36] A systematic variation of the electron dose dependence (see the Supporting Information) shows that for exposures lower than 1 mC/cm^2 only short fibers are formed that coexist with islands, while exclusive fiber growth is observed for deposition at 320 K after exposure of 4 and 5 mC/cm^2. As with the X-ray irradiated samples, no fiber growth is observed for electron-irradiated KCl if the sample was exposed to air prior to DNTT deposition, demonstrating that air contact quenches the F-centers localized at the surface.

To analyze the fiber growth on irradiated KCl theoretically and understand the microscopic mechanism, the changes in adsorption geometry and substrate interaction of DNTT on a pristine and irradiated KCl surface (with an F-center) were analyzed in the frame of DFT calculations. Previous work revealed a stabilized adsorption of substituted benzene on F-centers of KCl surfaces, leading to a modified orientation geometry.[37] In analogy to the previous study, we evaluated the impact of the surface Cl vacancies on the growth mechanisms of the DNTT films by considering two different geometrical configurations where molecules stay perpendicular or lying flat on the surface, and by analyzing their interface with both pristine and defected KCl surfaces. First, with the objective of mimicking the first steps of crystal formation, we started our analysis by considering isolated DNTT molecules (only one molecule per unit cell, see Section S12 of the Supporting Information for more details) and described their interaction with the surface by computing their adsorption energies (E_{ads})

https://doi.org/10.1021/acsami.2c13934
ACS Appl. Mater. Interfaces 2022, 14, 46086−46094

by following the procedure explained in the Section 4, see Table 1.

Table 1. Computed Interaction Energies (in eV) between an Isolated DNTT Molecule or a Layer of Molecules with the Pristine and Defected KCl Surfaces together with the Corresponding Energy Change due to the Presence of the Vacancy $(\Delta E)_{\text{F-cent}}$[a]

	isolated		layers	
surface	$(E_{ads})_{up}$	$(E_{ads})_{down}$	$(E_{ads})_{up}$	$(E_{ads})_{down}$
pristine	−0.27	−1.68	−0.25	−0.27
defected	−0.32	−1.93	−0.31	−0.33
$(\Delta E)_{\text{F-cent}}$	−0.05	−0.25	−0.05	−0.06

[a]The suffix up/down is employed to denote those interfaces where DNTT molecules are standing up/lying down on the surface, i.e., with (001)/(120) orientations in the case of crystalline layers. The values given for the layers are normalized by the number of molecules.

Not surprisingly, isolated DNTT molecules lying flat on the KCl surfaces are more stable (larger absolute E_{ads} values) with respect to those molecules standing perpendicular to the surface due to their more pronounced van der Waals interactions. Nonetheless, this difference in energy $(\Delta E_{ads})_{\text{up-down}}$ is more marked (~by 0.2 eV) in the case of the defected surfaces, which demonstrates that the energetic barrier that one needs to overcome to keep the molecules perpendicular to the surface is higher when Cl vacancies are present. Actually, Cl vacancies promote a remarkable stabilization for both molecular configurations (denoted $(\Delta E)_{\text{F-cent}}$ in Table 1) which amounts to 0.05 and 0.25 eV for the standing-up and lying-down DNTT geometries, respectively. This enhancement of the interaction originates from an increase in the overlapping charge densities of the KCl surface and DNTT molecule at the interface that is prompted by the presence of the vacancy, as it is shown in Figure 4a,b. Very interestingly, the large vacancy-triggered stabilization experienced by DNTT molecules adsorbed parallel to the surface can be attributed to the enhanced electrostatic interactions between the F-centers and the electronegative sulfur atoms from the DNTT core. This result is evidenced by the localized interfacial charge transfer around the molecular core which is observed in the presence of defects (Figure 4d), which contrasts with the highly delocalized charge transfer along the whole molecular backbone for the pristine surfaces (Figure 4c). A similar stabilization effect was reported due to the interaction between F-centers and the oxygen and nitrogen heteroatoms present in aromatic molecules adsorbed on defected KCl surfaces.[37] In a second stage, we have computed the adhesion energies between a layer of DNTT molecules standing up or lying flat and the pristine and defective KCl surface, as explained in Section S12 of the Supporting Information. In this case, we do not recover the extra stabilization provided by the Cl vacancy when the layer of molecules is adsorbed flat on the surface. This indicates that the intermolecular interactions within the layer dominate and prevent reaching the exact geometry by maximizing the interaction with the Cl vacancy for one molecule of the cluster. Moreover, there is no major difference between the total adhesion energies for the two molecular orientations. Once the crystal has started to grow, there is thus no energy gain when changing the orientation of the crystal from lying flat to standing up molecules to compensate the interaction with the F-center. Therefore, we can conclude that F-centers lead to a stabilization of the very first interfacial DNTT molecules that are recumbently oriented. These stabilized molecules serve as template for the further crystallization process, as it was found before also for heteromolecular stacks,[38] and finally yield (120)- and (12$\bar{1}$)-oriented crystalline fibers. In the absence of defects, (001)-oriented films with upright molecular orientation are energetically favored with respect to the minimization of the surface free energy.

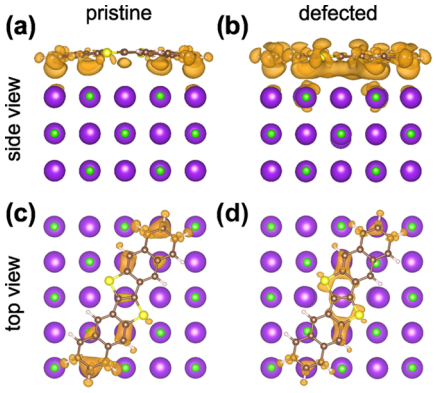

Figure 4. Side (a, b) and top (c, d) views of the interfacial charge density difference ($\Delta\rho = \rho_{\text{KCl/DNTT}} - \rho_{\text{KCl}} - \rho_{\text{DNTT}}$) plots for a DNTT molecule adsorbed on (a, c) the pristine and (b, d) defected (i.e., Cl vacancy) KCl surfaces. For the sake of better visualization, different isovalues were used to plot the isosurfaces: 3×10^{-4} a.u. for (a, b) and 4×10^{-4} and 8×10^{-4} a.u. for (c, d), respectively. The corresponding charge density difference plots for the standing-up molecular geometries are reported in Figure S16.

We note that the interaction between the inorganic substrate and molecular adlayers is sometimes described mesoscopically considering the substrate's surface energy as a key parameter. While this continuum description is applicable to polymeric or polycrystalline films on amorphous substrates where specific interactions between molecules and special substrate lattice sites are absent, the presence of chlorine vacancies at specific lattice sites on KCl(100) surfaces requires microscopic modeling of such localized electrostatic interaction with the nucleating DNTT molecules beyond the concept of surface energies. Interestingly, there are also more homogeneous electrostatic stabilizations of molecular adlayers that depend on the specific surface orientation. In previous work, it was demonstrated that in-plane surface dipoles on a ZnO(10$\bar{1}$0) surface stabilize a recumbent molecular orientation of sexiphenylene films, while without such additional electrostatic interaction, like on ZnO(0001), films with an upright molecular orientation are formed.[39,40]

Now that the mechanism of fiber formation in DNTT films by F-centers has been identified, we turn to the lateral structuring of molecular films. For this purpose, the KCl(100) surface is first irradiated with electrons through a metallic shadow mask to generate F-centers only in defined surface areas, and then the entire substrate is subsequently coated with DNTT. As depicted in Figure 5a−c, the optical micrographs confirm that characteristic DNTT fibers are only formed over the irradiated KCl regions, while islands are present on nonirradiated regions. In the optical micrographs, the island regions appear bluish and the fiber areas greyish brown, which is due to increased light scattering from the fiber regions as they exhibit larger film roughness. It should be noted that such

https://doi.org/10.1021/acsami.2c13934
ACS Appl. Mater. Interfaces 2022, 14, 46086−46094

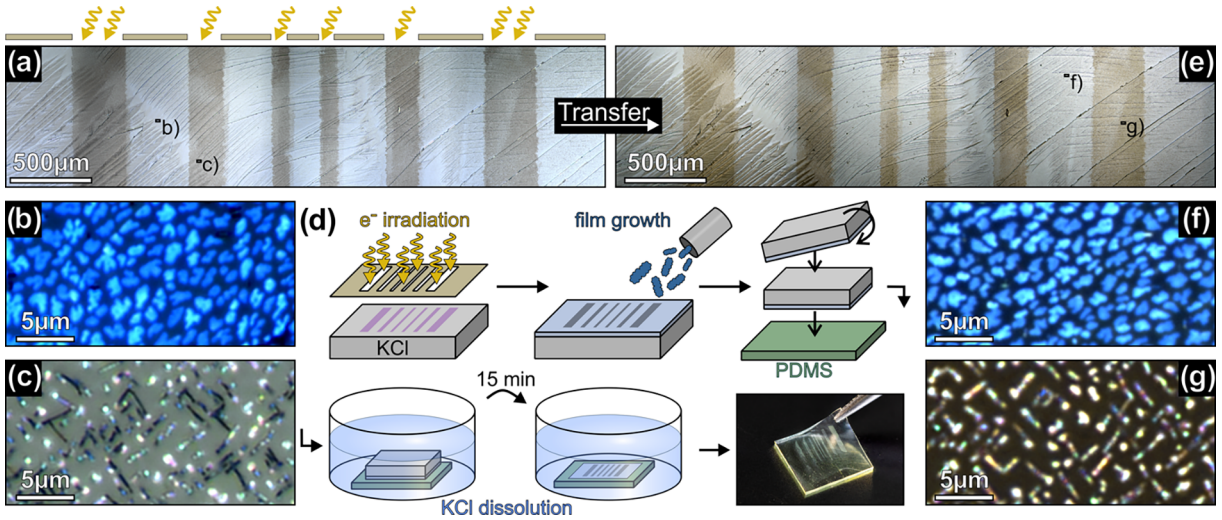

Figure 5. (a) Optical micrograph of a nominally 10 nm thick DNTT film grown at 320 K on KCl(100) that was electron-irradiated through a stripe mask prior to the film deposition together with magnified optical micrographs of films formed on (b) nonirradiated and (c) electron-irradiated KCl regions. (d) Schematic sketch of the wet transfer process of structured DNTT films from KCl to PDMS substrates. (e–g) Optical micrograph of the transferred structured DNTT films on PDMS.

F-center-induced patterning is not limited to small areas, but can also be applied to large areas, as demonstrated by the film pattern shown in Figure 5a, which extends over 4 mm. Electrons also offer the advantage that any F-center template pattern can be written by an electron beam analogously to that used in electron beam lithography techniques.[41] On the other hand, it should be noted that this F-center mediated patterning is not limited to the use of electrons and can also be achieved by X-rays.

Although the method presented here allows for lateral patterning and control of molecular orientation, it appears to be of limited value since it requires the use of KCl substrates, or other alkali halides in which F-centers can also be generated. However, the KCl as well as other alkali halide samples can be dissolved in water, which enables their use as growth templates followed by a wet transfer of the grown DNTT films onto other substrates. Details on such a wet transfer of thick DNTT films (about 50 nm) grown on pristine and homogeneously irradiated KCl(100) substrates onto SiO_2 (i.e., oxidized Si wafer) by dissolving KCl in water are provided in the Supporting Information (Figure S2). Actually, the X-ray diffractograms presented in Figure 1c were recorded for DNTT films that have been wet-transferred to SiO_2, since the overlap of the $(200)_{KCl}$ reflection with the $(120)_{DNTT}$ and $(12\bar{1})_{DNTT}$ reflections hampers a detailed analysis of the organic film orientation. A comparison of X-ray diffractograms of the DNTT films recorded before and after transfer (see the Supporting Information, Figure S2) shows that the film orientation remains intact and is not affected by the wet transfer.

Finally, we show that even very thin (10 nm) and structured films that were discussed before (cf. Figure 5a–c) can also be transferred intact. As such thin films partly consist of noncontiguous fibers, we use PDMS as target substrate and apply a transfer scheme that is well established for the transfer of CVD-grown 2D materials.[42,43] As sketched in Figure 5d, the (structured) DNTT film is first dipped in liquid PDMS and left undisturbed until the PDMS elastomer is cured (without thermal annealing). Afterward, the KCl/DNTT/PDMS lamination stack is placed into distilled water to dissolve the KCl growth template. After complete KCl dissolution (that takes approximately 15 min), the DNTT film is transferred onto a flexible and transparent PDMS substrate. The optical overview image presented in Figure 5e shows that structured DNTT films can be transferred using this method, with the DNTT island and fiber structures fully preserved, as confirmed by high-resolution micrographs shown in Figure 5f,g.

3. CONCLUSIONS

The lithographic top-down structuring methods established for inorganic materials cannot be readily applied to organic materials due to their sensitivity to radiation so that the microstructuring of organic films must be based on bottom-up approaches. Since such molecular materials are van der Waals bound, this approach requires a thorough understanding of intermolecular and molecule-substrate interactions. Here we show that the balance of these interactions can be manipulated in a controlled manner by surface-localized F-centers generated by electron irradiation of alkali halide substrates, which controls the morphology and molecular orientation of the subsequently grown film. For the examined organic semiconductor DNTT, we demonstrate that coalesced islands of upright oriented molecules and jagged fibers of recumbent molecules are formed on pristine and irradiated KCl substrates, respectively. These different morphologies are rationalized by a DFT-based analysis that shows that interfacial recumbently oriented DNTT molecules are stabilized due to the electrostatic interaction between the electronegative sulfur atoms of DNTT and the chlorine vacancies of irradiated samples. Despite rather different crystalline orientations and morphologies, both film structures are epitaxial since the F-centers are not randomly distributed but are located on the surface lattice of the alkali halide substrate.

The identified mechanism is neither restricted to DNTT nor to KCl but is applicable also to other molecules with electron-rich heteroatoms or side groups as well as other alkali halides. Additionally, structural properties such as the crystalline phase or epitaxial alignment of organic films can be tuned by choosing alkali halide substrate of different lattice constants,[14,44–46] showing the great potential of the usage of F-

https://doi.org/10.1021/acsami.2c13934
ACS Appl. Mater. Interfaces 2022, 14, 46086–46094

centers as a versatile tool to control the structural properties and epitaxial alignment of organic films. On the other hand, the knowledge gained here calls for some caution when fabricating organic functional films on alkali halide substrates, since electron or X-ray irradiation prior to molecular beam deposition should be avoided to rule out potentially undesirable film orientations that compromise the structural order achieved on pristine substrates—an effect that has yet not been taken into consideration.

The potential of the newly introduced approach to fabricate laterally structured films with molecular orientation control was demonstrated by spatially selective irradiated substrates using shadow masks prior to organic film deposition. Furthermore, the water solubility of the alkali halide growth substrates allows wet transfer of patterned films to any other non-water-soluble substrate even to flexible elastomeric substrates, hence demonstrating the versatility of the patterning method presented here.

4. METHODOLOGY

4.1. Experimental Details. The KCl(100) substrates with a surface area of about 1 cm^2 were prepared by cleaving slices of about 2 mm from single-crystal rods (Korth Kristalle GmbH). Immediately after cleavage, the samples were transferred into a high-vacuum system using a load-lock system and heated to 650 K in vacuum to desorb residual adsorbates and to heal possible surface defects.[29] The DNTT (Sigma-Aldrich, purity >99%) films were grown under high-vacuum conditions by molecular beam deposition from resistively heated Knudsen cells. The growth rate was held constant at 3 Å/min as monitored by quartz crystal microbalance. Before DNTT film deposition, some KCl samples were additionally irradiated by electrons (E = 250 eV, dose 5 mC/cm^2) using the electron gun of the LEED system (Omicron) or by synchrotron X-ray light using the HE-SGM beamline of the electron storage ring BESSY II (for details, see the Supporting Information) to create surface and bulk F-centers. For the DNTT film transfer, polydimethylsiloxane (PDMS) films were prepared using a Sylgard 184 silicone elastomer kit. The morphology of the organic films was characterized by atomic force microscopy (AFM, Agilent SPM 5500), operated under ambient conditions in tapping mode using MikroMasch cantilevers with a spring constant of 40 N/m (f_{res} = 325 kHz) and a tip radius of 8 nm. Additional information was obtained by optical microscopy (Nikon Eclipse LV-FMA, equipped with a sensitive DS-Ri2 camera) and scanning electron microscopy (SEM, JEOL JSM-7500F, operated at an electron beam energy of 5−10 keV). To avoid charging of the insulating KCl samples, they were covered by a 10 nm thick platinum layer prior to the SEM measurements. Note, that after SEM measurements, the coated samples were not used for any other measurements. The crystalline phase and orientation of the DNTT films were analyzed by X-ray diffraction (XRD), using a Bruker D8 Discovery diffractometer with monochromatized Cu Kα radiation (λ = 1.542 Å) and a sensitive one-dimensional LynxEye silicon strip detector.

4.2. Computational Details. All theoretical calculations related to the KCl/DNTT interfaces were conducted in the framework of DFT using the Perdew−Burke−Ernzerhof (PBE) functional,[47] including periodic boundary conditions (PBC) and the Grimme's D3 dispersion model[48] to take into account the van der Waals interactions. In view of the large number of atoms involved in these calculations (>2000), for the geometry relaxations, we relied on a combination of a Gaussian and plane wave basis set especially suitable for high parallel architectures, as implemented in the CP2K package.[49] These calculations were performed with a Double-ζ Valence Polarized (DZVP) basis set and an energy cut-off for the auxiliary plane wave basis equal to 500 Ry, whereas the core electrons were described by means of Goedecker−Teter−Hutter (GTH) pseudopotentials.[50] The computation of the charge densities was carried out within a pseudopotential/plane wave formalism, as implemented in the Quantum-Espresso (QE) suite program.[51] Ultrasoft pseudopotentials from the QE libraries were used for the description of the core electrons, whereas energy cutoffs equal to 25 and 200 Ry were employed for the kinetic energy and the charge density, respectively. Due to the large dimensions of the systems under study, all calculations were carried out only at the Γ point of the Brillouin zone. The E_{ads} magnitudes have been computed by employing the following formula

$$E_{ads} = \frac{E_{KCl/DNTT} - E_{KCl} - E_{DNTT}}{n} \quad (1)$$

Here, $E_{KCl/DNTT}$ represents the energy of the full system, while E_{KCl} and E_{DNTT} are the energies of the KCl slab and the DNTT molecular layer, respectively, in their relaxed geometries, and n is the number of DNTT molecules per unit cell.

The modeling of the habit of the isolated bulk DNTT crystal has been carried out by employing the Morphology module of the BIOVIA Materials Studio package.[52] In practice, the surface free energies for all crystal faces are calculated from eq 2 on the basis of the X-ray crystal structure

$$E_{surf} = \frac{1}{2}\lim_{M\to 7}\frac{E_{latt}(M) - E_{slice}(M)}{A_{hkl}} \quad (2)$$

where $E_{latt}(M)$ is the energy of an M layer thick slab inside the infinite crystal, $E_{slice}(M)$ is the energy of an M layer thick slab in vacuum, and A_{hkl} is the surface area of a plane with Miller indices (hkl).

The reported equilibrium morphology corresponds to the crystal habit that minimizes the surface energy and is represented using a Wulff plot. Note that the (negligible) polar surface correction has been estimated with a fixed substrate thickness of 7 layers. All calculations were performed with the COMPASSII force field which already proved successful to simulate morphologies of small organic conjugated molecules.[53,54] The Ewald summation method has been used to estimate the electrostatic interactions. The attachment energy was considered as the energy per molecule released when one slice of thickness d_{hkl} crystallizes onto a crystal face {hkl}, as it is defined in the original work of Hartman.[55]

■ ASSOCIATED CONTENT

Supporting Information

The Supporting Information is available free of charge at https://pubs.acs.org/doi/10.1021/acsami.2c13934.

Additional structural characterizations of DNTT films and crystals; micrographs of the temperature-dependent DNTT film morphology; LEED measurements on pristine and irradiated KCl; DNTT films prepared on X-ray-irradiated KCl together with complementary calculations on the DNTT crystal morphology and on

https://doi.org/10.1021/acsami.2c13934
ACS Appl. Mater. Interfaces 2022, 14, 46086−46094

the adsorption of DNTT molecules on (irradiated) KCl (PDF)

AUTHOR INFORMATION

Corresponding Author

Gregor Witte − *Fachbereich Physik, Philipps-Universität Marburg, 35032 Marburg, Germany;* orcid.org/0000-0003-2237-0953; Email: gregor.witte@physik.uni-marburg.de

Authors

Darius Günder − *Fachbereich Physik, Philipps-Universität Marburg, 35032 Marburg, Germany;* orcid.org/0000-0001-7969-5519

Valentin Diez-Cabanes − *Laboratory for Chemistry of Novel Materials, University of Mons (UMONS), BE-7000 Mons, Belgium; Laboratoire de Physique et Chimie Théoriques (LPCT), Université de Lorraine & CNRS, F-54000 Nancy, France;* orcid.org/0000-0002-6234-2749

Andrea Huttner − *Fachbereich Physik, Philipps-Universität Marburg, 35032 Marburg, Germany;* orcid.org/0000-0002-7441-077X

Tobias Breuer − *Fachbereich Physik, Philipps-Universität Marburg, 35032 Marburg, Germany;* orcid.org/0000-0002-9962-9444

Vincent Lemaur − *Laboratory for Chemistry of Novel Materials, University of Mons (UMONS), BE-7000 Mons, Belgium;* orcid.org/0000-0001-8601-286X

Jérôme Cornil − *Laboratory for Chemistry of Novel Materials, University of Mons (UMONS), BE-7000 Mons, Belgium*

Complete contact information is available at: https://pubs.acs.org/10.1021/acsami.2c13934

Notes

The authors declare no competing financial interest.

ACKNOWLEDGMENTS

The authors acknowledge the financial support provided by the German Science Foundation (Deutsche Forschungsgemeinschaft, DFG) project-ID 223848855-SFB 1083 "Structure and Dynamics of Internal Interfaces" within the project A2 and thank the Helmholtz-Zentrum Berlin (electron storage ring BESSY II) for provision of synchrotron radiation at the beamline HE-SGM as well as Daniel Bischof, Yurii Radiev, and Fazeel Zohair for their support at the beamline. They also thank Michael Hellwig for his assistance with the SEM measurements. D.G. gratefully acknowledges financial support by the Cusanuswerk. V.D.-C. is grateful to the COMETE (COnception in silico de Matériaux pour l'EnvironnemenT et l'Energie) and "Fire Light" ("Photo-bio-active molecules and nanoparticles") projects for the financial support, being both grants co-funded by the European Union under the program FEDER-FSE Lorraine et Massif des Vosges 2014-2020. J.C. is an FNRS Research Director. The computational resources are provided by the Consortium des Équipements de Calcul Intensif (CECI) funded by the Belgian National Fund for Scientific Research (F.R.S.-FNRS) under Grant 2.5020.11; the Tier-1 supercomputer of the Wallonie-Bruxelles Federation, infrastructure funded by the Walloon Region under the grant agreement n°1117545; and the mésocentre EXPLOR of Université de Lorraine (Project 2018CPMXX0602).

REFERENCES

(1) Klauk, H. *Organic Electronics*; Wiley, 2006.

(2) Bredas, J.-L.; Marder, S. R. *The WSPC Reference on Organic Electronics: Organic Semiconductors*; World Scientific, 2016; Vol. *1*.

(3) Menard, E.; Meitl, M. A.; Sun, Y.; Park, J.-U.; Shir, D. J.-L.; Nam, Y.-S.; Jeon, S.; Rogers, J. A. Micro- and Nanopatterning Techniques for Organic Electronic and Optoelectronic Systems. *Chem. Rev.* **2007**, *107*, 1117−1160.

(4) Kang, B.; Lee, W. H.; Cho, K. Recent Advances in Organic Transistor Printing Processes. *ACS Appl. Mater. Interfaces* **2013**, *5*, 2302−2315.

(5) Aleeva, Y.; Pignataro, B. Recent Advances in Upscalable Wet Methods and Ink Formulations for Printed Electronics. *J. Mater. Chem. C* **2014**, *2*, 6436−6453.

(6) Wang, W.; Du, C.; Zhong, D.; Hirtz, M.; Wang, Y.; Lu, N.; Wu, L.; Ebeling, D.; Li, L.; Fuchs, H.; Chi, L. Control over Patterning of Organic Semiconductors: Step-Edge-Induced Area-Selective Growth. *Adv. Mater.* **2009**, *21*, 4721−4725.

(7) Pick, A.; Witte, G. Patterned Growth of Organic Semiconductors: Selective Nucleation of Perylene on Self-Assembled Monolayers. *Langmuir* **2016**, *32*, 8019−8028.

(8) Gaucci, P.; Fruehauf, N.; Ilchmann, A.; Polzinger, B.; Eberhardt, W.; Kueck, H. Organic Thin Film Transistors on Back Molded Plastic Foil. *Flexible Printed Electron.* **2018**, *3*, No. 015008.

(9) García, J. F.; Höfle, S.; Zhang, M.; Dlugosch, J.; Friedrich, T.; Wagner, S.; Colsmann, A. OLED Luminaires: Device Arrays with 99.6% Geometric Fill Factor Structured by Femtosecond Laser Ablation. *ACS Appl. Mater. Interfaces* **2017**, *9*, 37898−37904.

(10) Li, L.; Hirtz, M.; Wang, W.; Du, C.; Fuchs, H.; Chi, L. Patterning of Polymer Electrodes by Nanoscratching. *Adv. Mater.* **2010**, *22*, 1374−1378.

(11) Balzer, F.; Rubahn, H.-G. Laser-Controlled Growth of Needle-Shaped Organic Nanoaggregates. *Nano Lett.* **2002**, *2*, 747−750.

(12) Pithan, L.; Beyer, P.; Bogula, L.; Zykov, A.; Schäfer, P.; Rawle, J.; Nicklin, C.; Opitz, A.; Kowarik, S. Direct Photoalignment and Optical Patterning of Molecular Thin Films. *Adv. Mater.* **2017**, *29*, No. 1604382.

(13) Yang, J.; Yan, D.; Jones, T. S. Molecular Template Growth and its Applications in Organic Electronics and Optoelectronics. *Chem. Rev.* **2015**, *115*, 5570−5603.

(14) Breuer, T.; Witte, G. Epitaxial Growth of Perfluoropentacene Films with Predefined Molecular Orientation: A Route for Single-Crystal Optical Studies. *Phys. Rev. B* **2011**, *83*, No. 155428.

(15) Dreher, M.; Günder, D.; Zörb, S.; Witte, G. Van der Waals Bound Organic Semiconductor/2D-Material Hybrid Heterosystems: Intrinsic Epitaxial Alignment of Perfluoropentacene Films on Transition Metal Dichalcogenides. *Chem. Mater.* **2020**, *32*, 9034−9043.

(16) Jones, A. O. F.; Chattopadhyay, B.; Geerts, Y. H.; Resel, R. Substrate-Induced and Thin-Film Phases: Polymorphism of Organic Materials on Surfaces. *Adv. Funct. Mater.* **2016**, *26*, 2233−2255.

(17) Yamamoto, T.; Takimiya, K. Facile Synthesis of Highly Pi-Extended Heteroarenes, Dinaphtho2,3-b:2′,3′-fchalcogenopheno3,2-bchalcogenophenes, and their Application to Field-Effect Transistors. *J. Am. Chem. Soc.* **2007**, *129*, 2224−2225.

(18) Zschieschang, U.; Ante, F.; Kälblein, D.; Yamamoto, T.; Takimiya, K.; Kuwabara, H.; Ikeda, M.; Sekitani, T.; Someya, T.; Nimoth, J. B.; Klauk, H. Dinaphtho[2,3-b:2′,3′-f]thieno[3,2-b]-thiophene (DNTT) Thin-Film Transistors with Improved Performance and Stability. *Org. Electron.* **2011**, *12*, 1370−1375.

(19) Głowacki, E. D.; Irimia-Vladu, M.; Kaltenbrunner, M.; Gsiorowski, J.; White, M. S.; Monkowius, U.; Romanazzi, G.; Suranna, G. P.; Mastrorilli, P.; Sekitani, T.; Bauer, S.; Someya, T.; Torsi, L.; Sariciftci, N. S. Hydrogen-Bonded Semiconducting Pigments for Air-Stable Field-Effect Transistors. *Adv. Mater.* **2013**, *25*, 1563−1569.

(20) Hamaguchi, A.; Negishi, T.; Kimura, Y.; Ikeda, Y.; Takimiya, K.; Bisri, S. Z.; Iwasa, Y.; Shiro, T. Single-Crystal-Like Organic Thin-Film Transistors Fabricated from Dinaphtho2,3-b:2′,3′-fthieno3,2-

bthiophene (DNTT) Precursor-Polystyrene Blends. *Adv. Mater.* **2015**, *27*, 6606−6611.
(21) Shioya, N.; Eda, K.; Shimoaka, T.; Hasegawa, T. Hidden Thin-Film Phase of Dinaphthothienothiophene Revealed by High-Resolution X-Ray Diffraction. *Appl. Phys. Express* **2020**, *13*, No. 095505.
(22) Breuer, T.; Karthäuser, A.; Klemm, H.; Genuzio, F.; Peschel, G.; Fuhrich, A.; Schmidt, T.; Witte, G. Exceptional Dewetting of Organic Semiconductor Films: The Case of Dinaphthothienothiophene (DNTT) at Dielectric Interfaces. *ACS Appl. Mater. Interfaces* **2017**, *9*, 8384−8392.
(23) Käfer, D.; Wöll, C.; Witte, G. Thermally Activated Dewetting of Organic Thin Films: The Case of Pentacene on SiO2 and Gold. *Appl. Phys. A* **2009**, *95*, 273−284.
(24) Briseno, A. L.; Mannsfeld, S. C. B.; Ling, M. M.; Liu, S.; Tseng, R. J.; Reese, C.; Roberts, M. E.; Yang, Y.; Wudl, F.; Bao, Z. Patterning Organic Single-Crystal Transistor Arrays. *Nature* **2006**, *444*, 913−917.
(25) Dreher, M.; Bischof, D.; Widdascheck, F.; Huttner, A.; Breuer, T.; Witte, G. Interface Structure and Evolution of Dinaphthothienothiophene (DNTT) Films on Noble Metal Substrates. *Adv. Mater. Interfaces* **2018**, *5*, No. 1800920.
(26) Götzen, J.; Käfer, D.; Wöll, C.; Witte, G. Growth and Structure of Pentacene Films on Graphite: Weak Adhesion as a Key for Epitaxial Film Growth. *Phys. Rev. B* **2010**, *81*, No. 085440.
(27) Breuer, T.; Maßmeyer, T.; Mänz, A.; Zoerb, S.; Harbrecht, B.; Witte, G. Structure of Van Der Waals Bound Hybrids of Organic Semiconductors and Transition Metal Dichalcogenides: The Case of Acene Films on MoS2. *Phys. Status Solidi RRL* **2016**, *10*, 905−910.
(28) Günder, D.; Watanabe, K.; Taniguchi, T.; Witte, G. Van der Waals Bound Organic/2D Insulator Hybrid Structures: Epitaxial Growth of Acene Films on hBN(001) and the Influence of Surface Defects. *ACS Appl. Mater. Interfaces* **2020**, *12*, 38757−38767.
(29) Thommen, K. Über die Erhöhung der Röntgen-Verfärbbarkeit von KCl-Kristallen durch Vorbestrahlung mit Ionisierenden Strahlen. *Z. Naturforsch. A* **1961**, *16*, 992−1001.
(30) Mitchell, P. V.; Wiegand, D. A.; Smoluchowski, R. Formation of F Centers in KCl by X Rays. *Phys. Rev.* **1961**, *121*, 484−498.
(31) Sibley, W. A.; Sonder, E. Hardening of KCl by Electron and Gamma Irradiation. *J. Appl. Phys.* **1963**, *34*, 2366−2370.
(32) Ueta, M.; Kondo, Y.; Hirai, M.; Yoshinari, T. F Center Formation in KCl Crystals by Pulsed Electron Beam at 80°K. *J. Phys. Soc. Jpn.* **1969**, *26*, 1000−1006.
(33) Soul, P. B. F-Centre Saturation Phenomena in KCl During Low-Energy Electron Irradiation. *Phys. Status Solidi A* **1970**, *42*, 801−812.
(34) Mikhailov, M. M.; Ardyshev, V. M. Build-Up of F and M Color Centers in KCl Single Crystals Under Combined Electron and Proton Irradiation. *Phys. Solid State* **1998**, *40*, 1823−1826.
(35) Friedenberg, A.; Shapira, Y. Electron-Induced Sputtering of KCl and NaCl. *J. Phys. C: Solid State Phys.* **1982**, *15*, 4763−4768.
(36) Stawinski; Bauer. Alkali Halide Layers on W(110): Electron-Stimulated Desorption of Ions, Structure, and Composition. *Phys. Rev. B* **1993**, *47*, 12820−12831.
(37) Häfner, M.; Hochheim, M.; Bredow, T. Chemistry with F Centers: Reduction of Organic Molecules on the Defective Potassium Chloride(100) Surface. *J. Phys. Chem. C* **2020**, *124*, 12606−12616.
(38) Breuer, T.; Witte, G. Controlling Nanostructures by Templated Templates: Inheriting Molecular Orientation in Binary Heterostructures. *ACS Appl. Mater. Interfaces* **2015**, *7*, 20485−20492.
(39) Della Sala, F.; Blumstengel, S.; Henneberger, F. Electrostatic-Field-Driven Alignment of Organic Oligomers on ZnO Surfaces. *Phys. Rev. Lett.* **2011**, *107*, No. 146401.
(40) Blumstengel, S.; Glowatzki, H.; Sadofev, S.; Koch, N.; Kowarik, S.; Rabe, J. P.; Henneberger, F. Band-Offset Engineering in Organic/Inorganic Semiconductor Hybrid Structures. *Phys. Chem. Chem. Phys.* **2010**, *12*, 11642−11646.
(41) Vieu, C.; Carcenac, F.; Pépin, A.; Chen, Y.; Mejias, M.; Lebib, A.; Manin-Ferlazzo, L.; Couraud, L.; Launois, H. Electron Beam Lithography: Resolution Limits and Applications. *Appl. Surf. Sci.* **2000**, *164*, 111−117.
(42) Reina, A.; Son, H.; Jiao, L.; Fan, B.; Dresselhaus, M. S.; Liu, Z.; Kong, J. Transferring and Identification of Single- and Few-Layer Graphene on Arbitrary Substrates. *J. Phys. Chem. C* **2008**, *112*, 17741−17744.
(43) Li, X.; Cai, W.; An, J.; Kim, S.; Nah, J.; Yang, D.; Piner, R.; Velamakanni, A.; Jung, I.; Tutuc, E.; Banerjee, S. K.; Colombo, L.; Ruoff, R. S. Large-Area Synthesis of High-Quality and Uniform Graphene Films on Copper Foils. *Science* **2009**, *324*, 1312−1314.
(44) Möbus, M.; Karl, N.; Kobayashi, T. Structure of Perylene-Tetracarboxylic-Dianhydride Thin Films on Alkali Halide Crystal Substrates. *J. Cryst. Growth* **1992**, *116*, 495−504.
(45) Schwabegger, G.; Djuric, T.; Sitter, H.; Resel, R.; Simbrunner, C. Morphological and Structural Investigation of Sexithiophene Growth on KCl (100). *Cryst. Growth Des.* **2013**, *13*, 536−542.
(46) Balzer, F.; Sun, R.; Parisi, J.; Rubahn, H.-G.; Lützen, A.; Schiek, M. Epitaxial Growth of a Methoxy-Functionalized Quaterphenylene on Alkali Halide Surfaces. *Thin Solid Films* **2015**, *597*, 104−111.
(47) Perdew; Burke; Ernzerhof. Generalized Gradient Approximation Made Simple. *Phys. Rev. Lett.* **1996**, *77*, 3865−3868.
(48) Grimme, S.; Antony, J.; Ehrlich, S.; Krieg, H. A Consistent and Accurate Ab Initio Parametrization of Density Functional Dispersion Correction (DFT-D) for the 94 Elements H-Pu. *J. Chem. Phys.* **2010**, *132*, No. 154104.
(49) Hutter, J.; Iannuzzi, M.; Schiffmann, F.; VandeVondele, J. cp2k: Atomistic Simulations of Condensed Matter Systems. *Wiley Interdiscip. Rev.: Comput. Mol. Sci.* **2014**, *4*, 15−25.
(50) Goedecker; Teter; Hutter. Separable Dual-Space Gaussian Pseudopotentials. *Phys. Rev. B* **1996**, *54*, 1703−1710.
(51) Giannozzi, P.; Baroni, S.; Bonini, N.; Calandra, M.; Car, R.; Cavazzoni, C.; Ceresoli, D.; Chiarotti, G. L.; Cococcioni, M.; Dabo, I.; Dal Corso, A.; de Gironcoli, S.; Fabris, S.; Fratesi, G.; Gebauer, R.; Gerstmann, U.; Gougoussis, C.; Kokalj, A.; Lazzeri, M.; Martin-Samos, L.; Marzari, N.; Mauri, F.; Mazzarello, R.; Paolini, S.; Pasquarello, A.; Paulatto, L.; Sbraccia, C.; Scandolo, S.; Sclauzero, G.; Seitsonen, A. P.; Smogunov, A.; Umari, P.; Wentzcovitch, R. M. QUANTUM ESPRESSO: A Modular and Open-Source Software Project for Quantum Simulations of Materials. *J. Phys. Condens. Matter* **2009**, *21*, No. 395502.
(52) *Materials Studio*, BIOVIA;Dassault Systèmes, 2018.
(53) Schweicher, G.; Paquay, N.; Amato, C.; Resel, R.; Koini, M.; Talvy, S.; Lemaur, V.; Cornil, J.; Geerts, Y.; Gbabode, G. Toward Single Crystal Thin Films of Terthiophene by Directional Crystallization Using a Thermal Gradient. *Cryst. Growth Des.* **2011**, *11*, 3663−3672.
(54) Lemaur, V.; Bouzakraoui, S.; Olivier, Y.; Brocorens, P.; Burhin, C.; El Beghdadi, J.; Martin-Hoyas, A.; Jonas, A. M.; Serban, D. A.; Vlad, A.; Boucher, N.; Leroy, J.; Sferrazza, M.; Mouthuy, P.-O.; Melinte, S.; Sergeev, S.; Geerts, Y.; Lazzaroni, R.; Cornil, J.; Nysten, B. Structural and Charge-Transport Properties of a Liquid-Crystalline α,ω-Disubstituted Thiophene Derivative: A Joint Experimental and Theoretical Study. *J. Phys. Chem. C* **2010**, *114*, 4617−4627.
(55) Hartman, P. The Attachment Energy as a Habit Controlling Factor. *J. Cryst. Growth* **1980**, *49*, 166−170.

https://doi.org/10.1021/acsami.2c13934
ACS Appl. Mater. Interfaces 2022, 14, 46086−46094